1-1-2013

Controlled fabrication of Si nanoparticles on graphene sheets for Li-ion batteries

Shenmin Zhu
Shanghai Jiao Tong University

Chengling Zhu
Shanghai Jiao Tong University

Jun Ma
University of South Australia, jma@uow.edu.au

Qing Meng
University of Wollongong, qm982@uowmail.edu.au

Zaiping Guo
University of Wollongong, zguo@uow.edu.au

See next page for additional authors

Controlled fabrication of Si nanoparticles on graphene sheets for Li-ion batteries

Abstract

A new route is presented for the synthesis of Si nanoparticle/Graphene (Si-Gr) composite by a sonochemical method and then magnesiothermic reduction process. During the process, silica particles were firstly synthesized and deposited on the surface of graphene oxide (SiO2-GO) by ultrasonic waves, subsequent low-temperature magnesiothermic reduction transformed SiO 2 to Si nanoparticles in situ on graphene sheets. The phase of the obtained materials was influenced by the weight ratio of Mg to SiO 2-GO. With the optimized ratio of 1 : 1, we can get Si nanoparticles on Gr sheets, with the average particle size of Si around 30 nm. Accordingly, the resultant Si-Gr with 78 wt% Si inside delivered a reversible capacity of 1100 mA h g-1, with very little fading when the charge rates change from 100 mA g-1 to 2000 mA g-1 and then back to 100 mA g-1. Thus, this strategy offers an efficient method for the controlled synthesis of Si nanoparticles on Gr sheets with a high rate performance, attributing to combination of the nanosized Si particles and the graphene. 2013 The Royal Society of Chemistry.

Keywords

graphene, nanoparticles, li, sheets, si, batteries, ion, fabrication, controlled

Disciplines

Engineering | Science and Technology Studies

Publication Details

Zhu, S., Zhu, C., Ma, J., Meng, Q., Guo, Z., Yu, Z., Lu, T., Li, Y., Zhang, D. & Lau, W. Ming. (2013). Controlled fabrication of Si nanoparticles on graphene sheets for Li-ion batteries. RSC Advances, 3 (17), 6141-6146.

Authors

Shenmin Zhu, Chengling Zhu, Jun Ma, Qing Meng, Zaiping Guo, Ziyong Yu, Tao Lu, Yao Li, Di Zhang, and Woon Ming Lau

RSC Advances

RSC Publishing

PAPER

View Article Online
View Journal | View Issue

Cite this: *RSC Advances*, 2013, **3**, 6141

Controlled fabrication of Si nanoparticles on graphene sheets for Li-ion batteries

Shenmin Zhu,*[a] Chengling Zhu,[a] Jun Ma,[b] Qing Meng,[c] Zaiping Guo,[c] Ziyong Yu,[a] Tao Lu,[a] Yao Li,[a] Di Zhang*[a] and Woon Ming Lau[d]

Received 23rd November 2012,
Accepted 13th February 2013

DOI: 10.1039/c3ra22989k

www.rsc.org/advances

A new route is presented for the synthesis of Si nanoparticle/Graphene (Si–Gr) composite by a sonochemical method and then magnesiothermic reduction process. During the process, silica particles were firstly synthesized and deposited on the surface of graphene oxide (SiO_2–GO) by ultrasonic waves, subsequent low-temperature magnesiothermic reduction transformed SiO_2 to Si nanoparticles *in situ* on graphene sheets. The phase of the obtained materials was influenced by the weight ratio of Mg to SiO_2–GO. With the optimized ratio of 1 : 1, we can get Si nanoparticles on Gr sheets, with the average particle size of Si around 30 nm. Accordingly, the resultant Si–Gr with 78 wt% Si inside delivered a reversible capacity of 1100 mA h g^{-1}, with very little fading when the charge rates change from 100 mA g^{-1} to 2000 mA g^{-1} and then back to 100 mA g^{-1}. Thus, this strategy offers an efficient method for the controlled synthesis of Si nanoparticles on Gr sheets with a high rate performance, attributing to combination of the nanosized Si particles and the graphene.

1. Introduction

Silicon (Si) has long been considered as a promising anode material for rechargeable Li-ion batteries (LIBs), owing to its abundance in nature, low Li insertion potential (<0.5 V *vs.* Li/Li^+) and high theoretical lithium storage at 4200 mA h g^{-1}.[1] However, it suffers an over 300% volume expansion during charge/discharge cycling, causing severe capacity fading, which severely limits its applications. A number of strategies were thus proposed to minimize its expansion, which include decreasing the dispersion phase size,[2] alloying it with metals,[3] creating Si/inactive-component composites,[4] employing nanostructured Si materials[1b,5] and coating its surface with carbon;[6] of these, the most effective approach is to disperse nanoscale Si in a carbon matrix, where carbon acts as both a structural buffer and an electroactive material.[7] Si nanoscale is extremely important for anode materials because nanoparticles exhibit much lower particle–particle distance, in which the stress caused by the volume change can be accommodated more readily than that in bulk silicon.[8] A nanocomposite anode, which has been prepared by pyrolyzing a mixture of phenol–formaldehyde resin with commercial nanoentities of Si and MWCNTs, showed a reversible charge capacity of 711 mA h g^{-1} after 20 cycles; this high capacity was mainly caused by the morphological stability of the nanocomposite due to the good carbon resiliency and MWCNT electrical conductivity.[9]

In comparison with MWCNTs, graphene has far higher electronic conductivity, mechanical property and surface area (>2600 m^2 g^{-1}).[10] When graphene is compounded with nanoparticles to produce anode materials for LIB, graphene stacking may be prevented due to the presence of these particles; on the other hand, electrically conductive graphene could accommodate the large volume change during Li insertion/extraction processes to maintain good electronic contact between nanoparticles and graphene.[11] Therefore, graphene-based composites have started attracting extensive research interest in the development of advanced LIB.

Owing to its abundance in nature, low Li insertion potential and high theoretical lithium storage, Si-based materials have been compounded with graphene to produce LIB anode candidates, by simply mixing SiO_2 nanoparticles with graphene oxide (GO) followed by thermal reduction.[12] To obtain a homogeneous dispersion of Si nanoparticles, diazonium chemistry was adopted to produce covalent bonding between graphene and the nanoparticles.[13] The covalent linkages between the Si nanoparticles and graphene sheets are considered to contribute to the resultant high electrochemical performance; however, its application is thwarted by (i) the complex process with successively diazotizing two amines of p-phenylenediamine and (ii) the use of hazardous solvent of HF and CH_3CN. Moreover, the Si nanoparticles used in these

[a]*State Key Lab of Metal Matrix Composites, Shanghai Jiao Tong University, 800 Dongchuan Road, Shanghai, 200240, P. R. China. E-mail: smzhu@sjtu.edu.cn; zhangdi@sjtu.edu.cn; Fax: +86-21-34202749; Tel: +86-21-34202584*
[b]*School of Advanced Manufacturing & Mechanical Engineering, University of South Australia, South Australia, Australia*
[c]*Institute for Superconducting and Electronic Materials, University of Wollongong, Wollongong, Australia*
[d]*Beijing Computational Science Research Center, Beijing, 100084, P. R. China. Chengdu Green Energy and Green Manufacturing Technology R&D CenterSichuan, 610207, P. R. China*

examples are generally commercial products with diameters of over 100 nm. To get Si nanoparticles with smaller size, magnesiothermic reduction of three-dimensional silica microassemblies into silicon replicas were developed in 2007.[14] This method is attractive for the SiO_2 as a precursor is environmentally friendly. Nevertheless, to the best of our knowledge, no report concerning about the fabrication of Si/graphene composites from SiO_2/graphene has been reported. There are two obstacles existing in the synthesis of Si particles from SiO_2 on the surface of graphene sheets: (i) how to control the fabrication of SiO_2 on the graphene sheet, and (ii) how to cost-effectively transform SiO_2 into Si nanoparticles.

In this work, we cost-effectively fabricate Si/graphene nanocomposites (Si–Gr) by a simple sonochemical approach followed by a magnesiothermic reduction process. Through identification of various fabrication variables, we synthesize Si nanoparticles of controllable size that are uniformly dispersed on the surface of graphene sheets. As an anode material for LIB, these nanocomposites demonstrate a remarkable performance in rate capability.

2. Experimental

2.1 Preparation of graphene oxide

Graphene oxide (GO) was prepared by the Hummers method. In specifics, 2 g graphite and 1 g $NaNO_3$ were mixed and then added into 50 mL H_2SO_4 in a 250 mL flat-bottom flask placed in an ice bath. After the mixture had been stirred for 30 min, 6 g $KMnO_4$ power was slowly added using 10 min. Then the ice bath was replaced by an oil bath. The mixture was stirred at 15 °C for 2 h; it increased to 40 °C, at which the mixing was kept for 1 h. The next step was to add 90 mL H_2O to the pasty mixture slowly. Finally, 30 mL of 5% H_2O_2 was added to the mixture and increase the temperature to 95 °C, at which the mixing was kept for 1h. For purification, the mixture was centrifuged with deionized water and dried under vacuum at 60 °C for 24 h.

2.2 Preparation of SiO_2/graphene oxide composites

SiO_2/graphene oxide composites (SiO_2–GO) were synthesized by the sonochemical reaction of tetraethylorthosilicate (TEOS) in the presence of GO. A calculated amount of the as-prepared GO (0.4 g) was dispersed in 78 mL ethanol by an ultrasonic treatment. Then 0.0025 g hexadecyltrimethyl-ammonium bromide (CTAB), 16 mL H_2O and 6 mL TEOS were added into the above mixture under ultrasonic irradiation for 3 h. After that, 2 mL hydrazine hydrate was added, followed by stirring at 85 °C for 10 h. The obtained composite was filtered and dried under vacuum at 60 °C for 24 h.

2.3 Preparation of Si/graphene composites

A Si/graphene composite was synthesized *via* a magnesiothermic reduction. 0.1 g SiO_2–GO and 0.12 g magnesium were placed on the opposite sides of a porcelain boat, which was loaded into a steel tube with an Ar atmosphere. After flowing Ar for 1 h to minimize the air content, the tube was sealed. The tube was heated to 700 °C with an Ar atmosphere. Magnesia was removed by washing the heated sample with HCl solution (1 M). This produces a Si/graphene composite.

2.4 Characterization

The synthesized samples were characterized by X-ray diffraction (XRD) using a Rigaku/max 2550VL/PC system operated at 35 kV and 200 mA with Cu-Kα radiation (λ = 1.5406 Å), at a scan rate of 5° min^{-1} and a step size of 0.050° in 2θ. Nitrogen adsorption measurements at 77 K were performed using an ASAP2020 volumetric adsorption analyzer, after the samples had been vacuumed for 8 h in the degas port of the adsorption apparatus. Raman spectroscopy was measured by Renishaw inVia Raman Microscope. Fourier transform-infrared measurements (FT-IR) were recorded on KBr pellets with a PE Paragon 1000 spectrophotometer. X-Ray photoelectron spectra (XPS) were collected on a physical electronics PHI5400 using Mg K radiation as X-ray source. All the spectra were corrected with the C 1s (285.0 eV) band. Diffuse reflectance electronic spectra were measured with a Perkin–Elmer 330 spectrophotometer equipped with a 60 mm Hitachi integrating sphere accessory. Transmission electron microscopy (TEM), selected area electron diffraction (SAED) and energy dispersive spectrometer (EDS) were carried out on a JEOL 2010 microscope at 200 kV. Scanning electron microscopy (SEM) was performed on a JEOL JSM-6360LV field emission microscope at an accelerating voltage of 15 kV. Thermal gravimetric analysis (TGA) was conducted on a PE TGA-7 instrument with a heating rate of 20 °C min^{-1}.

2.5 Electrochemical measurements

Electrochemical experiments were carried out in two-electrode Swagelok cells. The working anode was made by (i) mixing the composite with carbon black and binder (sodium carboxymethyl cellulose, CMC) at a mass ratio of 80 : 10 : 10, and (ii) spreading the mixture uniformly onto a copper foil of 12 mm in diameter, followed by drying in vacuum at 80 °C. Metallic lithium foil was used as counter electrode. The cells were assembled in an argon filled glove box (Mikrouna 1220/750). Metallic lithium foil was used as a counter electrode. The electrolyte was made of 1 M $LiPF_6$ dissolved in the mixture of ethylene carbonate (EC) and diethylenecarbonate (DEC) with a volume ratio of 1 : 1. Then, galvanostatical charge and discharge were carried out at a current density of 50 mA g^{-1} between 5 mV and 1.2 V and cyclic voltammograms (CV) were tested between 2.0 and 0 V at a scan rate of 0.2 mV s^{-1}. Rate performance was measured under the same condition at various currents.

3. Results and discussion

The synthesis of Si nanoparticles on the graphene sheets is described in Scheme 1. The GO sheets were first coated with silica by a sonochemical method to produce a SiO_2–GO composite. Both the matrix and dispersion phase were reduced by a thermal reduction process assisted with magnesium powders under Ar atmosphere at 650 °C. After

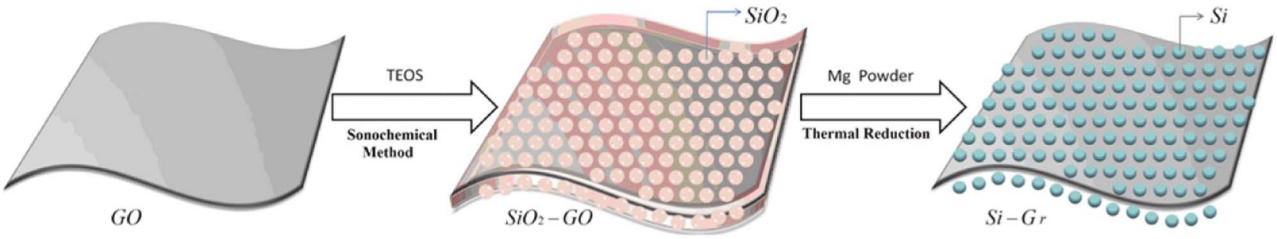

Scheme 1 Schematic fabrication of Si/graphene nanocomposite.

removal of magnesium compounds by acid etching, we produced a Si/graphene nanocomposite (Si–Gr).

During this process, three kinds of reactions occurred as below:

$$2Mg + SiO_2 \rightarrow 2MgO + Si \quad (1)$$

$$Si + C \rightarrow SiC \quad (2)$$

$$Si + 2Mg \rightarrow Mg_2Si \quad (3)$$

During the reduction process, Mg powders not only reduced SiO_2 to Si as described in eqn (1), but also produced MgO, SiC and Mg_2Si; of these products, MgO and Mg_2Si were removed by acid etching, implying the importance of the ratio of Mg to the nanocomposite on the component of the obtained samples. Thus, three weight ratios were investigated, including 1 : 1, 1 : 1.5 and 2 : 1.

Fig. 1 contains XRD patterns of the composites fabricated with these ratios. At the first ratio 1 : 1, it shows that after the magnesiothermic reduction, the amorphous graphene oxide and SiO_2 were converted to graphene and silicon, respectively, and Si exists as the main crystalline phase (JCPDF: 895012) with a small trace of SiC (Fig. 1a). With the ratio decreasing to 1 : 1.5, the phases of (111), (220) and (311) characteristic of Si were demonstrated; unfortunately, a diffraction at 21° corresponds to the phase of SiO_2, indicating an incomplete reduction of SiO_2. When the ratio increased to 2 : 1, the diffraction at 21° disappeared, explaining a complete reaction of SiO_2. However, the 35.6° diffraction is in agreement with the (111) reflection of *b*-SiC, and this is caused by the reaction between Si and the residual amorphous carbon from GO, the sample thus obtained is termed as SiC–Gr. In order to convert SiO_2 into Si completely without any formation of SiC, we chose 1 : 1 as the weight ratio in the fabrication of Si–Gr nanocomposite.

GO, SiO_2–GO composite and Si–Gr composite were firstly investigated by XRD measurement shown in Fig. 2. GO shows a broad diffraction at about 11° with a basal space of 0.86 nm. After ultrasonication where GO mixed with SiO_2, the diffraction was shifted to 10.5° with a reduced intensity, indicating the enlargement of the layer spacing of GO due to insertion of amorphous SiO_2. Through reduction by Mg powders, this diffraction disappears completely and a weak diffraction appears at about 26.5° attributing to the (002) layer of the graphite, which indicate a complete reduction from GO to graphene.[15] The broad character of the 26.5° diffraction implies the disordered stacking of graphene layers, different to the graphite structure.[16] The peaks at 2θ = 28.4, 47.3 and 56.1 corresponding to the planes of (111), (220) and (311)

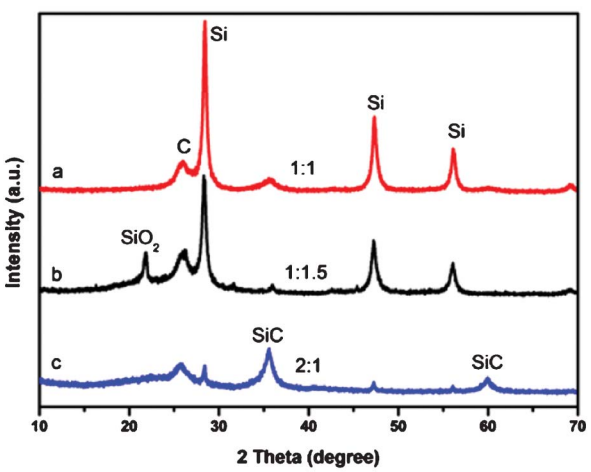

Fig. 1 XRD patterns of composites fabricated by the weight ratios of Mg to SiO_2–GO at (a) 1 : 1, (b) 1 : 1.5 and (c) 2 : 1.

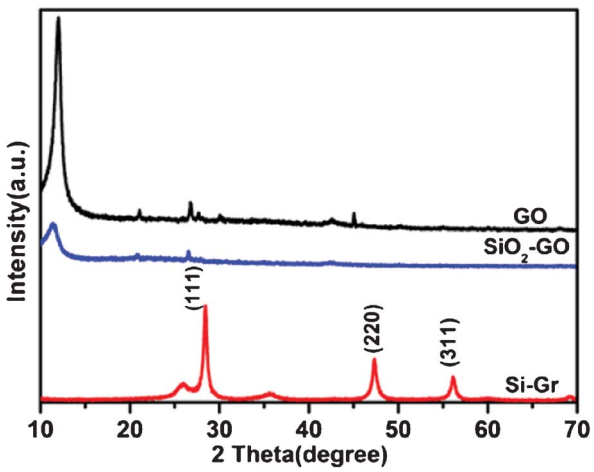

Fig. 2 XRD patterns of graphene oxide (GO), SiO_2–GO composite and Si/graphene (Si–Gr) composite.

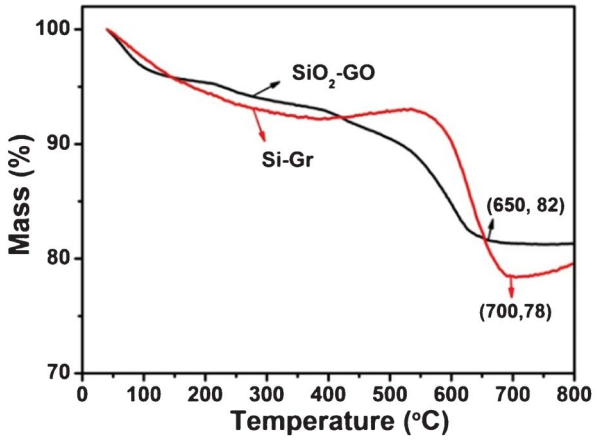

Fig. 3 TGA graphs of SiO_2–GO composite and Si–Gr composite.

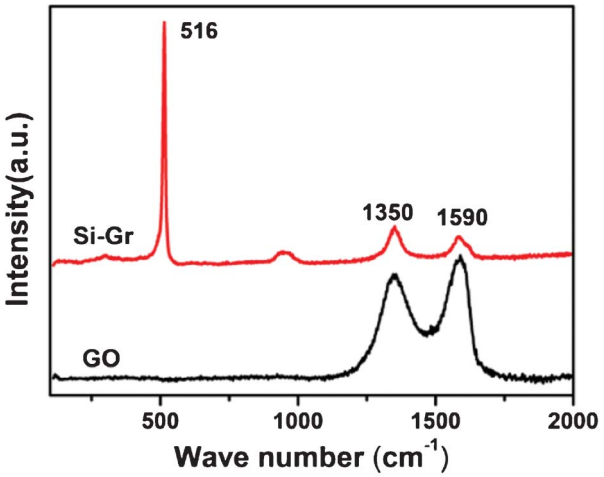

Fig. 4 Raman spectra of GO and Si–Gr composite.

characteristic of Si are clearly observed in graphene/Si composite. Calculating from the line width of the (220) diffraction, the average Si particle diameter is around 30 nm.

The Si loading was determined from weight loss by TGA in air. In Fig. 3, a distinct weight loss below 500 °C is seen for both composites, attributing to absorbed water and the organic groups of GO. It is worth mentioning that GO sheets, which were prepared by a modified Hummer's method, contain many carboxyl, hydroxyl and epoxy groups that act as the nucleation sites for growth of SiO_2 nanoparticles. Comparison of these two plots leads to a conclusion that Si–Gr composite has a higher thermal stability than SiO_2–GO composite. For Si–Gr composite, graphene begins to react with oxygen in air to generate CO_2 at 550 °C. A distinct weight increase detected after 700 °C should be caused by the oxidation of Si in air to produce SiO_2. Since the oxidation of Si powder in air is little under 680 °C and the samples were heated at 20 °C min^{-1}, it is reasonable to determine the content of Si in the Si–Gr composite from the largest weight loss at 22 wt%; that is, the Si fraction is 78 wt%.

Raman spectrum of the Si–Gr composite exhibits a maximal absorption at around 516 cm^{-1}, which corresponds to pure Si (Fig. 4). As expected, both composites contain D and G bands at around 1350 and 1595 cm^{-1}, respectively. The G-band is characteristic of graphitic sheets, corresponding to a well defined sp^2 carbon-type structure, whereas the D-band can be attributed to the presence of defects within the hexagonal graphitic structure. Thus a smaller I_D/I_G ratio indicates lower defects and disorders of the graphitized structures. Although previous studies point out that a thermal treatment reduces this ratio, the I_D/I_G ratio in this work increases from 0.9 for GO to 1.16 for Si–Gr composite. The higher I_D/I_G ratio is probably due to the existence of Si nanoparticles in the composite. Similar phenomenon has been reported by many others.[17]

The morphology of Si–Gr composite was revealed by SEM and TEM micrographs. GO shows a crumpled, stacked but expanded structure (Fig. 5a). After deposition with silica, many tiny particles are observed on the GO sheets in Fig. 5b. After reduction to produce Si–Gr composite, the sheets appear more crumpled, and pockets of void space are clearly visible (Fig. 5c). A great number of bright nanoscale crystalline Si particles are homogeneously coated on the sheets (Fig. 5d). The homogeneous dispersion of Si nanoparticles is favorable for the stable structure of the Si–Gr composite.

Fig. 6 shows typical TEM micrographs of Si–Gr composite. The graphene sheets and Si particles of 30 nm in diameter are clearly distinguished. These particles are deposited on the surface of graphene (Fig. 6c, d). The lattice fringe with spacing of around 0.31 nm shown in the high-resolution TEM images corresponds to the (111) plane of Si crystal (Fig. 6e).

Typical EDX pattern confirms the presence of Si and C elements in Si–Gr composite (Fig. 6f).

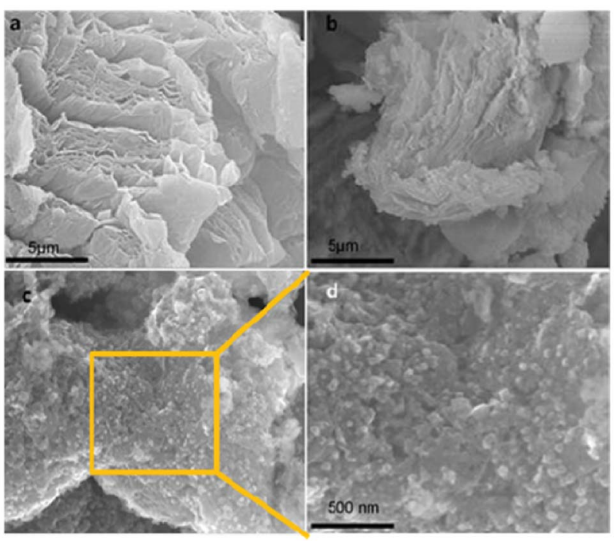

Fig. 5 SEM micrographs of (a) GO, (b) SiO_2–GO composite and (c, d) Si–Gr composite at different magnifications.

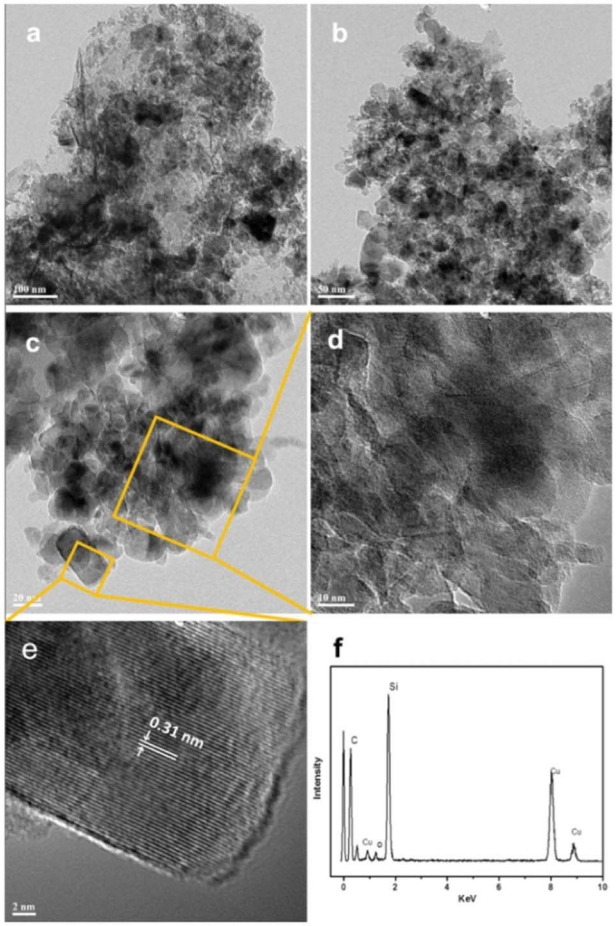

Fig. 6 (a–e) TEM micrographs in different resolutions and (f) EDX pattern of Si–Gr composite.

Electrochemical properties

A series of electrochemical measurements were carried out to study the Li storage properties of a half-cell configuration based on our Si–Gr composite. The cyclic voltammetry (CV) curves of cycles 1–4 were tested at a scan rate of 0.1 mV s^{-1} (Fig. 7). The process of lithium intercalation to graphene can be primarily divided into two stages: (i) from 0.4 to 0.1 V, lithium ions intercalate lightly to form 1.5- or 2-stage compounds (LiC_9 or LiC_{12}), and (ii) from 0.1 to 0 V, the ions intercalates deeply to form one-stage compound (LiC_6). In the following oxidation half-cycles, the peak of lithium de-intercalation from graphene emerged at around 0.34 V, followed by that of lithium extraction from Si. A characteristic peak for silicon delithiation appeared at approximately 0.5 V *versus* Li, which is consistent with the lithiation/delithiation of crystalline silicon reported previously.[13] In the first scanning cycle, there is a broad cathodic peak located at 0.62 V, which has disappeared since the second cycle; this phenomenon is attributed to the formation of a solid electrolyte interface (SEI) passivation layer on the surface of the composite electrode, due to the reaction of lithium with electrolyte.[18] Once the SEI layer is formed, it will be stable under subsequent lithium insertion and extraction cycles. Two anodic peaks located at

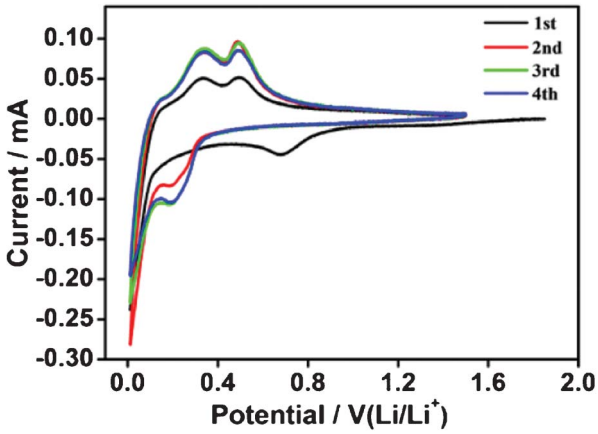

Fig. 7 Cyclic voltammograms of Si–Gr composite from cycle 1 to 4.

0.34 and 0.50 V, gradually evolving from the first scanning cycle, become more distinct after the fourth cycle, which corresponds to the extraction of lithium ions from the Si–graphene electrode. The multiple discharge peaks suggest the combined extraction of lithium ions from silicon and deintercalation from layered graphene. The results are well consistent with the data reported in the literature.[19]

Fig. 8 shows the initial charge–discharge voltage profiles of Si–Gr composite. When Li ions insert into the composite electrode during the first cycle, the voltage initially drops dramatically, and then experiences a slow decrease as shown in the potential plateau in Fig. 8. The plateau below 0.50 V may be due to the formation of Li–Si alloys, which coexist with Si as two-phase regions.

The composite demonstrates charge and discharge capacities at 1144 and 1674, in the first cycle, respectively, indicating a coulombic efficiency of 68%. However, high efficiency is achieved without a large irreversible capacity loss from the second cycle (as shown by the absence of plateau near 0.9 eV in Fig. 8). The high coulombic efficiency implies

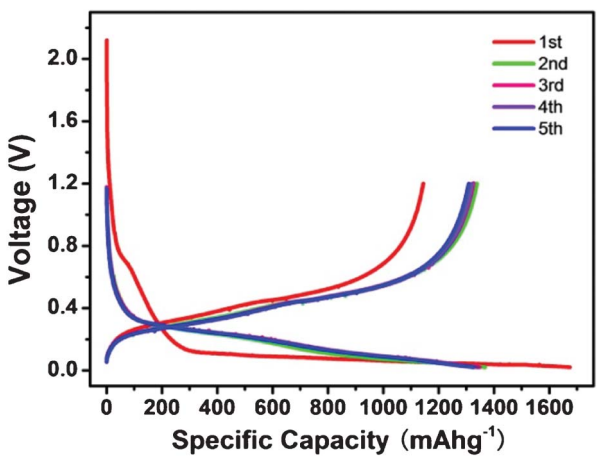

Fig. 8 Voltage profiles for selected cycles of Si–Gr at the current density of 100 mA g^{-1}.

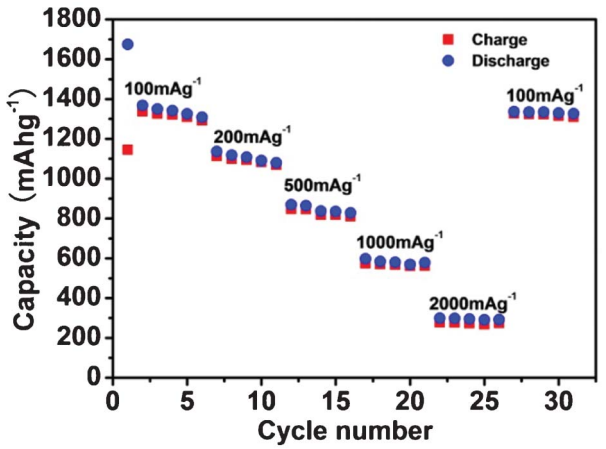

Fig. 9 Rate capabilities of Si–Gr at various currents.

much less decomposition of electrolyte in comparison with commercial carbonous electrode.

Fig. 9 shows rate capabilities of the composite electrodes at various currents. After testing the cell five cycles at a rate of 100 mA g^{-1}, the capacity reaches 1350 mA g^{-1}. The capacity reduces with increase in the rate, but it remains as high as 820 mA h g^{-1} at a rate of 500 mA g^{-1}. Even at a high current of 1000 mA g^{-1}, it delivers a high capacity of 580 mA h g^{-1}. To our satisfaction, the capacity recovers almost completely (1350 mA g^{-1}) when the discharge rate returns to 100 mA g^{-1} after 25 cycles. The profiles at various current densities indicate an excellent rate performance of the composite electrode. Since Si is known for its large theoretical lithium-storage capacity but less conductivity, graphene must take an indispensable role in improving the electrochemical performance of silicon electrode. As a result, high rate performance of LIBs is attributed from both Si phases and graphene matrix.

4. Conclusion

In summary, we have developed a novel method to synthesize a Si/graphene nanocomposite by using combination of sonochemistry and Mg-assisted reduction. The average size of Si nanoparticles is around 30 nm. The ratio of Mg to SiO_2 is critical to a complete conversion of SiO_2–GO precursors to Si–Gr composite. The resultant Si–Gr with 78 wt% Si inside delivered a reversible capacity of 1300 mAh g^{-1}, with very little fading when the charge rates change from 100 mA g^{-1} to 2000 mA g^{-1} and then back to 100 mA g^{-1}. These results suggest that electrodes of high-rate performance can be derived from our Si/graphene composite, provided that Si nanoparticles are well dispersed on graphene sheets, with improved electronic conductivity from graphene.

Acknowledgements

The authors gratefully acknowledge financial support for this research from the Morgan Crucible Company, the National Science Foundation of China (Nos. 51072117, 51171110), National Basic Research Program of China (973 Program, 2012CB619600, 2011CB922200), Shanghai Science and Technology Committee (0JC1407600) and the Research Fund for the Doctoral Program of Higher Education of China (20120073130001). We also thank the Shanghai Jiao Tong University (SJTU) Instrument Analysis Center.

References

1 (*a*) C. K. Chan, H. Peng, G. Liu, K. McIlwrath, X. F. Zhang, R. A. Huggins and Y. Cui, *Nat. Nanotechnol.*, 2008, **3**, 31; (*b*) H. Kim, B. Han, J. Choo and J. Cho, *Angew. Chem., Int. Ed.*, 2008, **47**, 10151.
2 H. Kim, M. Seo, M. H. Park and J. Cho, *Angew. Chem., Int. Ed.*, 2010, **49**, 2146.
3 V. A. Sethuraman, K. Kowolik and V. Srinivasan, *J. Power Sources*, 2011, **196**, 393.
4 N. Dimov, S. Kugino and M. Yoshio, *Electrochim. Acta*, 2003, **48**, 1579.
5 (*a*) B. Laik, L. Eude, J. P. Pereira-Ramos, C. S. Cojocaru, D. Pribat and E. Rouviere, *Electrochim. Acta*, 2008, **53**, 5528; (*b*) M. H. Park, M. G. Kim, J. Joo, K. Kim, J. Kim, S. Ahn, Y. Cui and J. Cho, *Nano Lett.*, 2009, **9**, 3844.
6 C. Martin, M. Alias, F. Christien, O. Crosnier, D. Belanger and T. Brousse, *Adv. Mater.*, 2009, **21**, 4735.
7 (*a*) C. Y. Du, M. Chen, L. Wang and G. P. Yin, *J. Mater. Chem.*, 2011, **21**, 15692; (*b*) L. W. Ji and X. W. Zhang, *Electrochem. Commun.*, 2009, **11**, 1146.
8 Y. Yu, L. Gu, C. B. Zhu, S. Tsukimoto, P. A. van Aken and J. Maier, *Adv. Mater.*, 2010, **22**, 2247.
9 Z. B. Zhou, Y. H. Xu, W. G. Liu and L. B. Niu, *J. Alloys Compd.*, 2010, **493**, 636.
10 K. S. Novoselov, E. McCann, S. V. Morozov, V. I. Fal'ko, M. I. Katsnelson, U. Zeitler, D. Jiang, F. Schedin and A. K. Geim, *Nat. Phys.*, 2006, **2**, 177.
11 S. L. Chou, J. Z. Wang, M. Choucair, H. K. Liu, J. A. Stride and S. X. Dou, *Electrochem. Commun.*, 2010, **12**, 303.
12 (*a*) J. K. Lee, K. B. Smith, C. M. Hayner and H. H. Kung, *Chem. Commun.*, 2010, **46**, 2025; (*b*) H. C. Tao, L. Z. Fan, Y. F. Mei and X. H. Qu, *Electrochem. Commun.*, 2011, **13**, 1332; (*c*) H. F. Xiang, K. Zhang, G. Ji, J. Y. Lee, C. J. Zou, X. D. Chen and J. S. Wu, *Carbon*, 2011, **49**, 1787.
13 S. N. Yang, G. R. Li, Q. Zhu and Q. M. Pan, *J. Mater. Chem.*, 2012, **22**, 3420.
14 Z. H. Bao, M. R. Weatherspoon, S. Shian, Y. Cai, P. D. Graham, S. M. Allan, G. Ahmad, M. B. Dickerson, B. C. Church, Z. T. Kang, H. W. Abernathy, C. J. Summers, M. L. Liu and K. H. Sandhage, *Nature*, 2007, **446**, 172.
15 C. Kim, K. S. Yang, M. Kojima, K. Yoshida, Y. J. Kim, Y. A. Kim and M. Endo, *Adv. Funct. Mater.*, 2006, **16**, 2393.
16 Y. S. Hu, R. Demir-Cakan, M. M. Titirici, J. O. Muller, R. Schlogl, M. Antonietti and J. Maier, *Angew. Chem., Int. Ed.*, 2008, **47**, 1645.
17 J. J. Guo, Y. Li, S. M. Zhu, Z. X. Chen, Q. L. Liu, D. Zhang, W. J. Moon and D. M. Song, *RSC Adv.*, 2012, **2**, 1356.
18 (*a*) B. Fang, M. S. Kim, J. H. Kim, S. Lim and J. S. Yu, *J. Mater. Chem.*, 2010, **20**, 10253; (*b*) M. S. Kim, B. Z. Fang, J. H. Kim, D. Yang, Y. K. Kim, T. S. Bae and J. S. Yu, *J. Mater. Chem.*, 2011, **21**, 19362.
19 J. Li and J. R. Dahn, *J. Electrochem. Soc.*, 2007, **154**, A156.

